PRELIMINARY

Abstract 6-398
ALEPH 99-060
CONF 99-035
July 1, 1999

Measurement of the $e^+e^- \to ZZ$ Production Cross Section at Centre-of-mass Energies of 183 and 189 GeV

ALEPH Collaboration
Contact person: Nikos Konstantinidis (N.Konstantinidis@cern.ch)

Abstract

The $e^+e^- \to ZZ$ cross sections at $\sqrt{s} = 182.7$ and 188.6 GeV have been measured using the ALEPH detector. The analysis covers all of the visible ZZ final states and yields cross section measurements of

$$\sigma_{ZZ}(182.7\ \mathrm{GeV}) = 0.11 \pm {}^{0.16}_{0.11}\,(\mathrm{stat.}) \pm 0.04\,(\mathrm{syst.})\,\mathrm{pb}$$

and

$$\sigma_{ZZ}(188.6\ \mathrm{GeV}) = 0.67 \pm 0.13\,(\mathrm{stat.}) \pm 0.04\,(\mathrm{syst.})\,\mathrm{pb},$$

consistent with the Standard Model expectations.

ALEPH contribution to the 1999 Summer Conferences

1 Introduction

The successful operation of LEP at and above the ZZ threshold in 1997 and 1998 allows for the first time, observation of a sizeable number of pair-produced resonant Z bosons. Within the Standard Model, the process $\mathrm{e^+e^-} \to \mathrm{ZZ}$ proceeds via the two "$\mathcal{NC}2$" diagrams which involve the t-channel exchange of an electron (see Figure 1).

This note describes a measurement of the ZZ $\mathcal{NC}2$ cross section at a centre-of-mass energy of 188.6 GeV using the ALEPH detector. It begins with a description of the detector and data samples, continues with a description of the event selections for the various final states, and concludes with the measured cross section. The same analysis was applied also on the 1997 ALEPH data, providing a measurement of the cross-section also at $\sqrt{s}$ =182.7 GeV.

2 ALEPH Detector

This section briefly describes the most salient features of the ALEPH detector. The interested reader can find detailed descriptions of the detector and its performance elsewhere [1, 2].

ALEPH is a cylindrically symmetric detector with its axis coincident with the beamline [3]. The three innermost detectors—a silicon microstrip detector, the inner tracking chamber, and the time-projection chamber (TPC)—measure the momentum of charged particles. With a 1.5 T axial magnetic field provided by a superconducting solenoidal coil, these detectors together achieve a transverse momentum resolution of $\delta p_t/p_t = 6 \times 10^{-4}\, p_t \oplus 5 \times 10^{-3}$ (p_t in GeV/c).

An electromagnetic calorimeter placed between the TPC and the superconducting coil identifies electrons and photons, and measures their energies with a resolution of $\delta E/E = 0.18/\sqrt{E}+0.009$ (E in GeV). This sampling calorimeter has a depth of 22 radiation lengths and consists of projective towers each of which subtends a solid angle of approximately $0.9^\circ \times 0.9^\circ$.

The iron return yoke is instrumented with 23 layers of streamer tubes and serves as a hadronic calorimeter. It is 7 interaction lengths deep and achieves an energy resolution of $\delta E/E = 0.85/\sqrt{E}$ for charged and neutral hadrons. Two additional layers of streamer tubes outside of the return yoke aid the identification of muons.

Two calorimeters at low polar angles extend the active region and measure the luminosity collected by the experiment. In 1997, ALEPH collected $56.8 \pm 0.3\ \mathrm{pb}^{-1}$ at $\sqrt{s} = 182.7\ \mathrm{GeV}$ and in 1998 $174.2 \pm 1.2\ \mathrm{pb}^{-1}$ at $\sqrt{s} = 188.6\ \mathrm{GeV}$. The uncertainty on the centre-of-mass energy is ± 50 MeV for both years.

An energy flow algorithm [2] combines the information from the tracking detectors and calorimeters and provides a list of reconstructed charged and neutral particles. It is these energy flow objects which are used in the analysis described below.

3 Simulation of Signal and Background

The YFSZZ Monte Carlo generator [4] provides a calculation of the expected Standard Model cross section for the $\mathcal{NC}2$ processes. The expected cross sections are 0.26 and 0.65 pb at $\sqrt{s} =$ 182.7 and 188.6 GeV, respectively. With a consistent set of electroweak parameters [5], three other Monte Carlo generators—PYTHIA [6], EXCALIBUR [7], and GRACE4F [8]—all agree with

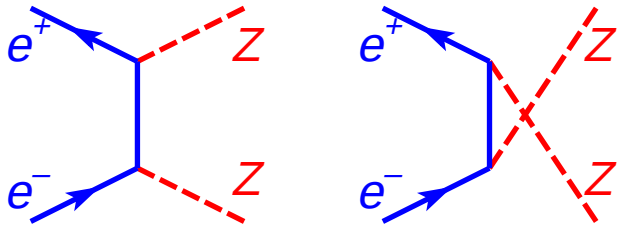

Figure 1: The t-channel Feynman diagrams show the ZZ $\mathcal{NC}2$ processes in the Standard Model.

the YFSZZ calculation within 2%; this can be considered the level of theoretical uncertainty on the $\mathcal{NC}2$ cross section determination.

Samples of ZZ events from the $\mathcal{NC}2$ and $\mathcal{NC}8$ [1] diagrams were generated with the PYTHIA Monte Carlo generator. The efficiencies were determined from the $\mathcal{NC}2$ sample. The difference between the $\mathcal{NC}2$ sample and the $\mathcal{NC}8$ sample was taken as background. This procedure accounts for any interference between the four-fermion diagrams. As a check, the analysis was repeated with samples generated with the EXCALIBUR Monte Carlo generator (see Section 6.1).

The KORALW [9] Monte Carlo generator was used to create a sample of the four-fermion backgrounds. To avoid double counting of the background, the overlap between this sample and the $\mathcal{NC}8$ ZZ samples was removed. The KORALW generator does not include the $\mathrm{e^+e^-} \to \mathrm{We}\nu$ and $\mathrm{e^+e^-} \to \mathrm{Ze^+e^-}$ processes with an untagged electron; consequently, additional samples for these processes were generated with the PYTHIA Monte Carlo generator.

For the two-fermion backgrounds, KORALZ generated the $\mathrm{e^+e^-} \to \mu^+\mu^-$ and $\mathrm{e^+e^-} \to \tau\tau$ events, BHWIDE [11] generated the $\mathrm{e^+e^-} \to \mathrm{e^+e^-}$ events, and PYTHIA generated the $\mathrm{e^+e^-} \to \mathrm{q\overline{q}}$ events. The two-photon backgrounds, $\gamma\gamma \to \mathrm{e^+e^-}$, $\gamma\gamma \to \mu^+\mu^-$, and $\gamma\gamma \to \tau\tau$, were generated with PHOT02 [12]. The process $\gamma\gamma \to \mathrm{hadrons}$ contributes negligibly to the background expectation after all of the analysis cuts and has not been simulated.

4 Event Selection

The analyses described below select events from all visible ZZ final states. While based on the Higgs boson search [13], these analyses have been tailored to the ZZ production process.

Two parallel analyses (with significant overlap) measure the ZZ production cross section. The first is an entirely cut-based analysis which uses the $\mathrm{q\overline{q}q\overline{q}}$, $\mathrm{q\overline{q}}\nu\overline{\nu}$, $\ell\ell\mathrm{XX}$, and $\ell^+\ell^-\nu\overline{\nu}$ channels. (Throughout this paper, the symbol ℓ denotes electrons and muons and X denotes quarks and leptons.) The second analysis (generically called the "NN" analysis) replaces the cut-based selections in the $\mathrm{q\overline{q}q\overline{q}}$ and $\mathrm{q\overline{q}}\nu\overline{\nu}$ channels with neutral networks and introduces an additional neural network to identify the $\tau\tau\mathrm{q\overline{q}}$ final state.

[1] these include, in addition to the diagrams of Figure 1, six other diagrams where one or both Z bosons are replaced by a photon

4.1 Leptonic Final States—ZZ $\rightarrow \ell\ell$XX

This analysis identifies those events in which one of the Z bosons decays into a pair of electrons or muons and the other decays into anything except neutrinos. Although the branching fraction of $\mathrm{Z} \rightarrow \ell\ell$ is small, the analysis benefits greatly from the high lepton identification efficiency and excellent mass resolution.

Selected events have four or more reconstructed charged particles. The total energy of all the charged particles must exceed 10% of the centre-of-mass energy. To remove radiative returns to the Z, the most energetic isolated photon in an event must have an energy less than $75\%\,\gamma_{\mathrm{peak}}$, where γ_{peak} is the most likely energy of the radiative return photon and is given by $\gamma_{\mathrm{peak}} = 0.5\,(\sqrt{s} - m_{\mathrm{Z}}^2/\sqrt{s})$.

Standard lepton cuts identify electron and muons in the event [14]. Electron energies are corrected for bremsstrahlung. To maintain a high selection efficiency, isolated charged particles are also considered as lepton candidates. The isolation is defined as the half-angle of the largest cone about a particle's direction which contains 5% or less of the event's total energy. Isolated particles have an isolation angle less than 10°. The pair of oppositely-charged lepton candidates with a mass closest to the Z mass is chosen as the $\mathrm{Z} \rightarrow \ell\ell$ pair. Only those pairs with at least one identified lepton are considered and $e\mu$ combinations are rejected. The mass of the lepton pair is corrected for final state radiation. Events in which the lepton pair contains an electron which is consistent with a photon conversion are rejected.

After the $\mathrm{Z} \rightarrow \ell\ell$ lepton pair has been selected, the DURHAM algorithm [15] clusters the remainder of the event into two jets; these jets must contain at least one charged particle. To remove $\mathrm{Ze^+e^-}$ events, the selection requires that the invariant mass of the two jets exceeds 15 GeV/c^2. In addition, the sum of the transverse momentum of the leptons with respect to the nearest jet must be greater than 20 GeV/c, where the nearest jet is the one which forms the smallest invariant mass with the lepton.

The process $\mathrm{WW} \rightarrow \mathrm{q\overline{q}}\,\ell\nu$ constitutes a large background when only one lepton is identified. The two W masses are calculated assuming that the event comes from this process. The mass of W which decays leptonically is calculated from the momentum of the identified lepton and the missing momentum. The invariant mass of the remainder of the event is the mass of the other W boson. Selected events have a sum of these masses less than 150 GeV/c^2 or a difference less than 20 GeV/c^2.

The mass of the lepton pair is used as the mass of the first Z candidate; that of the second candidate is the mass recoiling against the two leptons. Requiring that both Z masses be above 30 GeV/c^2 and the above cuts, the analysis selects 92 events from the data with 90.6 ± 1.4 expected from signal plus background. Figure 2 shows the invariant mass distribution of the two leptons.

To further reduce background levels, the two reconstructed masses must be consistent with the Z boson mass. As the leptonic invariant mass and recoil mass have different resolutions, an elliptical cut is defined using

$$r^2 = \left(\frac{m_{\ell\ell} - m_{\mathrm{Z}}}{\sigma_{m_{\ell\ell}}}\right)^2 + \left(\frac{m_{\mathrm{recoil}} - m_{\mathrm{Z}}}{\sigma_{m_{\mathrm{recoil}}}}\right)^2$$

where $\sigma_{m_{\ell\ell}} = 2.5$ and $\sigma_{m_{\mathrm{recoil}}} = 3.3$ GeV/c^2 are the approximate resolutions. Selected events have $r < 3$. The performance of this selection is summarized in Table 1.

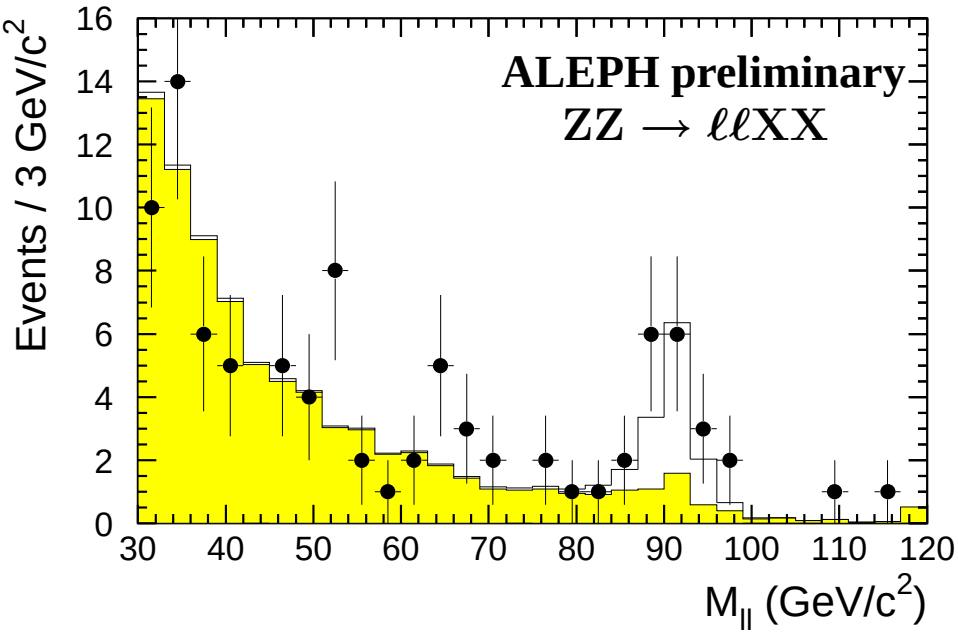

Figure 2: The distribution of masses for the $\ell\ell$XX channel. All cuts have been applied except the elliptical mass cut. The grey histogram shows the expected background and the hollow histogram, the expected signal.

Systematic uncertainties from lepton identification, tracking resolutions, and event kinematics have been studied. The total relative systematic uncertainty on the efficiency is 1.3% including uncertainties from limited Monte Carlo statistics. The relative uncertainty on the expected number of background events is 27%. Both uncertainties are dominated by limited Monte Carlo statistics.

4.2 Hadronic Final States—ZZ $\rightarrow \mathrm{q\overline{q}q\overline{q}}$

A total reconstructed energy near $\sqrt{s}$ and four distinct jets characterize events from the ZZ $\rightarrow \mathrm{q\overline{q}q\overline{q}}$ final state. This final state has the largest branching fraction, but also the largest background.

The cut-based and NN-based analyses of this channel use a common preselection. First, the event must contain 8 or more charged particles and the total energy of all charged particles must exceed 10% of the centre-of-mass energy.

The DURHAM algorithm clusters the event into four jets. To remove those events inconsistent with a four-jet topology, the value of the y_{cut} in the clustering algorithm which changes the event from a three-jet to four-jet event y_{34} must be large, $y_{34} > 0.004$. Additionally, all of the jets must contain at least one charged track.

Two additional cuts suppress events with initial state radiation. For events in which the initial state photon is not reconstructed, the longitudinal momentum of the event is constrained to be $|p_z| < 1.5\,(M_{\mathrm{vis}} - 90)$ with M_{vis} in GeV/c^2. Second, for those events in which the photon is inside the detector, the electromagnetic fraction of all of the jets must be smaller than 80%. This second cut also removes the $\mathrm{q\overline{q}e^+e^-}$ overlap with the leptonic channel described above.

4.2.1 Cut-based Selection

Three additional cuts augment the preselection for the cut analysis. The first two target $\mathrm{q\overline{q}}$ events: the thrust value of the event must be smaller than 0.9 and the sum of the four smallest angles between jets must be greater than 350°. The third cut reduces the overlap of $\mathrm{q\overline{q}}\mu^+\mu^-$ events between the $\mathrm{q\overline{q}q\overline{q}}$ and the $\ell\ell\mathrm{XX}$ selections. Accepted events have an invariant mass of the two most energetic muon candidates $m_{\mu\mu}$ less than 50 GeV/c^2 and satisfy the condition $p_1 + p_2 - m_{\mu\mu} < 35$ GeV/c, where p_1 and p_2 are the momenta of the two muons. For events with only one identified muon, this cut reduces to $p_1 < 35$ GeV/c. This cut negligibly affects the efficiency for the $\mathrm{q\overline{q}q\overline{q}}$ final state but rejects more than 97% of the $\mathrm{q\overline{q}}\mu^+\mu^-$ overlap. This cut also rejects a small fraction of the WW background.

After the above preselection, $1352 \pm 6\,(\mathrm{stat.})$ events are expected from the simulation, approximately 80% of which is from $\mathrm{WW} \to \mathrm{q\overline{q}q\overline{q}}$ events. In the data, 1219 events are observed; the apparent discrepancy has already been reported by ALEPH in the dedicated study of the $\mathrm{WW} \to \mathrm{q\overline{q}q\overline{q}}$ cross section measurement [17]. Its impact on the ZZ cross section measurement is studied in Section 6.2. The selection subsequently relies on the tagging of jets from b-quarks and on the dijet mass information. A four-constraint fit which imposes energy-momentum conservation [16] returns the dijet masses of the two Z bosons. A four variable neural network produces a value for each jet, η_i, which is near unity for b-jets and near zero for other jets [13].

The four-jet analysis is split into three sub-analyses—a $\mathrm{b\overline{b}b\overline{b}}$ selection, a $\mathrm{b\overline{b}q\overline{q}}$ selection, and a non-b-quark selection. When calculating the cross section, the two b-selections are treated as a single channel. The last sub-analysis replaces the b-tagging cuts with strict mass requirements to reject background while retaining efficiency for the majority of ZZ events ($\sim$62%) which do not contain b-quark jets.

The $\mathrm{b\overline{b}b\overline{b}}$ analysis selects events with high b-content, well-isolated jets, and large dijet masses. It requires that $y_{34} > 0.020$, that the sum of the dijet masses for at least one of the dijet combinations be above 170 GeV/c^2, and that $9.5\,y_{34} + \sum \eta_i > 3.1$ where the sum is over the four reconstructed jets.

For the other sub-selections the b-tagging requirements give way to tighter mass requirements. The mass information is contained in the quantities χ_W and χ_Z defined as

$$\chi_i^2 = \left(\frac{m_{12} + m_{34} - 2\,m_i}{\sigma_S^i}\right)^2 + \left(\frac{m_{12} - m_{34}}{\sigma_D^i}\right)^2$$

where i stands for W or Z. The contours of constant χ_W and χ_Z define two ellipses referred to as WW and ZZ ellipses throughout this section. The quantities σ_S^i and σ_D^i are the approximate resolutions of the sum and the difference of the dijet masses for the correct dijet combination, respectively. The values used for σ_S^i are 3 and 4 GeV/c^2 for the ZZ and the WW ellipse and 16 and 10 GeV/c^2 for σ_D^i.

The $\mathrm{b\overline{b}q\overline{q}}$ selection requires that at least one dijet combination falls inside the ZZ ellipse with $\chi_Z < 2.40$. For that combination, the dijet not containing the most poorly b-tagged jet must be compatible with $\mathrm{Z} \to \mathrm{b\overline{b}}$ in terms of b-tagging: $\min(\eta_1, \eta_2) > 0.20$ and $-\log_{10}(1 - \eta_1)(1 - \eta_2) > 1.50$.

Finally, the selection for $\mathrm{q\overline{q}q\overline{q}}$ events without b-jets raises the y_{34} cut to 0.006, tightens further the ZZ ellipse to $\chi_Z < 1.75$ and reduces the WW background by requiring that no dijet combination falls inside a WW ellipse with $\chi_W < 1.60$. To maintain the statistical indepen-

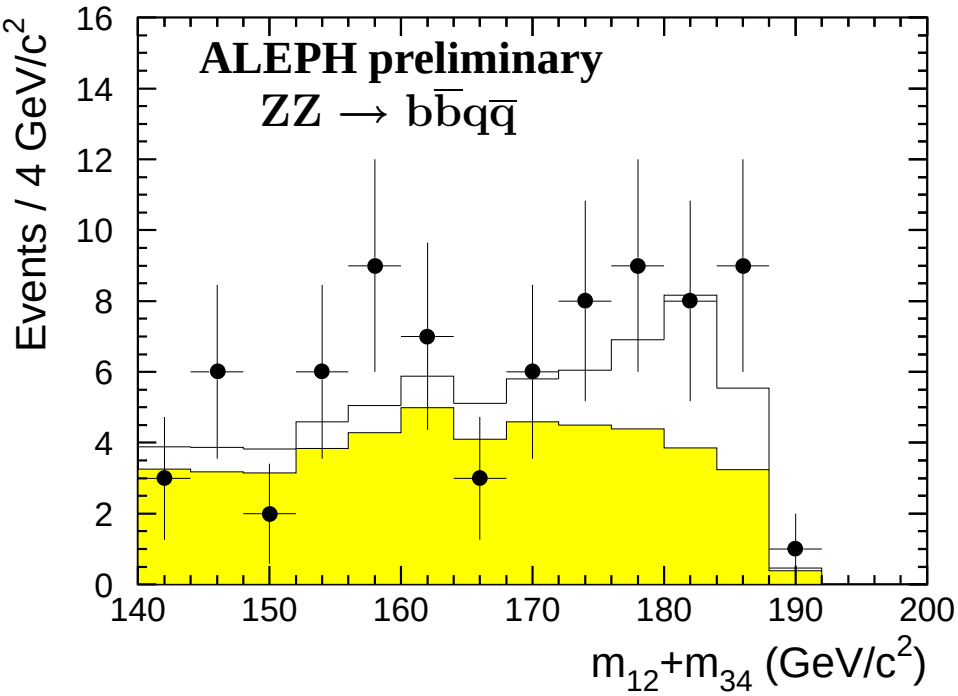

Figure 3: The distribution of masses for the $\mathrm{b\bar{b}b\bar{b}}$ and $\mathrm{b\bar{b}q\bar{q}}$ channels. All cuts have been applied except the elliptical mass cut. The hollow histogram is the contribution from the signal and the darker region that from the background.

dence of the b and non-b selections, this selection accepts only those events which have not been previously selected by the $\mathrm{b\bar{b}b\bar{b}}$ or $\mathrm{b\bar{b}q\bar{q}}$ cuts.

The performance of this selection is summarized in Table 1. Figure 3 shows the sum of the dijet masses for the $\mathrm{b\bar{b}b\bar{b}}$ and $\mathrm{b\bar{b}q\bar{q}}$ selections with the elliptical mass cut removed.

Although this selection does not specifically target $\tau\tau\mathrm{q\bar{q}}$ events, it nonetheless has a significant efficiency for these events ($\sim$17%). Consequently, the $\tau\tau\mathrm{q\bar{q}}$ selection described below is not included in the cut-based cross section measurement.

The systematic uncertainties in this channel include effects from the modelling of b-physics, from discrepancies in tracking between the simulation and the data, from discrepancies in reconstructed jet kinematics, from uncertainties in the Standard Model cross sections, from uncertainties in gluon splitting into heavy flavour, and from differences between the Standard Model Z branching fractions and those in the simulation. The total relative systematic uncertainties on the signal efficiencies are 1.7% and 1.3% for the b and non-b selections, respectively, with all of the sources having comparable contributions. The relative uncertainties for the background are 13% and 4%, dominated by the limited Monte Carlo statistics and jet corrections.

4.2.2 Neural Network Selection

A multivariate neural network is trained to select ZZ signal events from $\mathrm{q\bar{q}}$ and WW background events. During training, the network is presented with up to 6 dijet combinations per $\mathrm{q\bar{q}}$ or WW event, but only the correct dijet pairing for each signal event. If one Z decays to b-quarks, those jets are labelled 3 and 4, and the other two jets are labelled 1 and 2. Otherwise the jet labels are random. Reconstructed dijet masses are obtained using a four-constraint fit

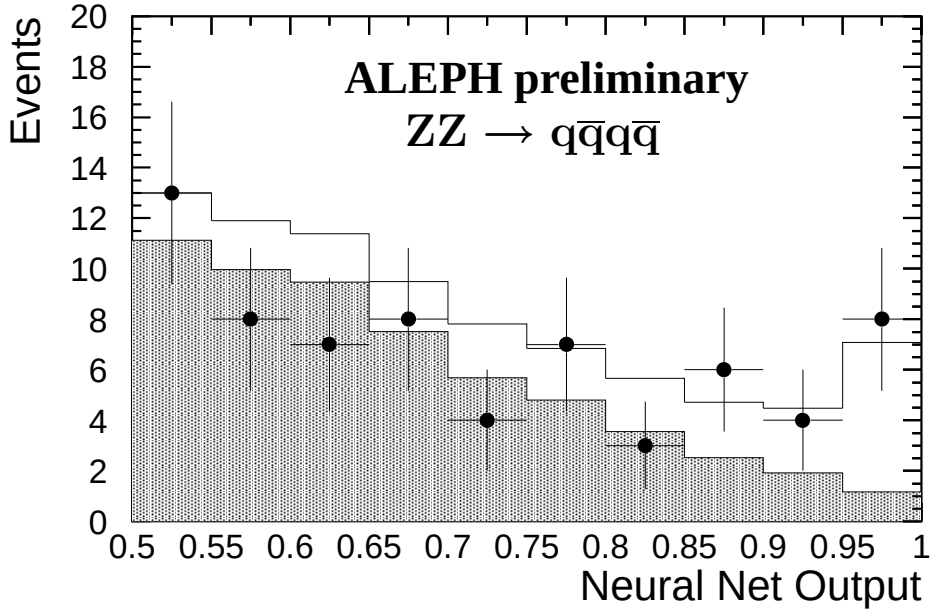

Figure 4: Neural network output from the $\mathrm{q\overline{q}q\overline{q}}$ selection for data and Monte Carlo simulation. The grey histogram shows the expected background, and the hollow histogram shows the expected $\mathcal{NC}2$ signal.

which requires energy-momentum conservation. Twenty-three event variables are used to discriminate specific signal and background features. In many cases, inclusion of similar variables in different combinations improves the neural network training.

The event variables y_{34}, thrust, and sphericity aid in selecting events with 4 separated jets. The missing energy and $\max\left(E_{\text{charged track}}/E_{\text{jet}}\right)$ the maximum scaled energy among all jets of the most energetic charged track in a jet, reject specifically semileptonic W decay.

A 6-variable b-tagging neural network [13] gives an output for each jet, and these variables are input as $\min(\eta_3, \eta_4)$, $(1-\eta_3)(1-\eta_4)$, and $\sum_{i=1}^{4}\eta_i$.

The reconstructed dijet masses are used to aid in selecting resonant ZZ production events. The mass combinations used as network inputs are m_{12}, m_{34}, and $(m_{12}-m_{34})^2+(m_{34}-m_{\mathrm{Z}})^2$. These variables perform the same function as an elliptical mass cut.

The jet boosted sphericity (calculated in the rest frame of the jet) of the Z candidate jets, the track multiplicity in the Z candidate jets, and the two lowest jet masses all help to separate light quark jets from gluon jets. The track multiplicity in this case is restricted to tracks with rapidity greater than 1.6.

The sum Θ of the four smallest inter-jet angles discriminates against $\mathrm{q\overline{q}}$ background events . The angular variable $\min\left(\cos\theta_{ij}+\cos\theta_{kl}\right)$ minimized over all jet combinations selects events with pairs of back-to-back jets. The event broadening variable

$$B=\min\left(\frac{\sum_{i=1}^{N^{\text{tracks}}}|p_{Ti}|}{\sum_{i=1}^{N^{\text{tracks}}}|p_i|}\right)$$

where p_T is calculated with respect to the thrust axis, also aids in this discrimination by rejecting $\mathrm{q\overline{q}}$ backgrounds with gluons that can lead to broad jets. Finally, the largest jet energy $E_{\max}$ and

the two smallest jet energies $E_{\min}$, $E_{\min 2}$ improve the overall discriminating power.

When more than one dijet combination is selected by the network, that pairing with the highest network output is used. The output of the neural network is shown in Fig. 4.2.2 for Monte Carlo simulation and for data. Only events with a network output greater than 0.7 are used in the cross section calculation. The performance of the selection is given in Table 1.

The total relative systematic uncertainty on the signal efficiency is 3%. No single effect dominates the uncertainty. The total relative uncertainties for the background are 11% ($\mathrm{q\overline{q}}$) and 7% (WW), dominated by kinematic effects and limited Monte Carlo statistics.

4.3 $\mathrm{Z} \rightarrow \mathrm{q\overline{q}}\nu\overline{\nu}$ Final States

Approximately 30% of the ZZ events have a $\mathrm{q\overline{q}}\nu\overline{\nu}$ final state characterized by missing and visible masses consistent with the Z mass.

Both the cut-based and NN-based analyses for this channel share a common preselection. First, events must contain more than 4 reconstructed charged particles and the total energy of all the charged particles must exceed 10% of the centre-of-mass energy. The plane perpendicular to the thrust axis divides the event into two hemispheres. These hemispheres are the "jets" used to calculate all of the kinematic quantities below. Both of the hemispheres must have a non-zero energy.

Events from the $\gamma\gamma \rightarrow \mathrm{hadrons}$ process, typically have a fraction of the total energy more than 30° degrees from the beamline smaller than 25% *and* a missing transverse momentum smaller than 5% of the centre-of-mass energy. The preselection removes these events.

Two additional cuts remove much of the background from events with initial state radiation. First, the magnitude of the longitudinal event momentum must be less than 50 GeV/c. Secondly, the missing mass must be greater than 50 GeV/c^2.

After the preselection, the background is dominated by $\mathrm{q\overline{q}}$ and WW events. Assuming the Standard Model cross section for ZZ production, 1533 ± 7 events are expected in good agreement with the 1493 actually observed in the data.

4.3.1 Cut-based Selection

The two-fermion background remaining after the preselection consists largely of $\mathrm{q\overline{q}}$ events with two or more initial state radiative photons. Requiring the acoplanarity A_{12} to be smaller than 0.08 removes much of this background. The acoplanarity of the two jets is defined as $A_{12} = (\hat{j}_1 \times \hat{j}_2) \cdot \hat{z}$ where $\hat{j}_i$ are the unit vectors along the jet directions.

Pairs of W bosons which subsequently decay as $\mathrm{WW} \rightarrow \tau\nu\,\mathrm{q\overline{q}}$ forms the other major background. For the case where the tau lepton decays leptonically, a cut on the isolation of identified leptons is made. The isolation is defined as the sum of the energy in a 30° cone around the lepton direction. Selected events have an isolation greater than 13 GeV. When the lepton from the tau decay is unidentified or the tau lepton decays hadronically, the previous cut is ineffective. For these cases, the analysis requires that the angle between the reconstructed charged particle with the highest momentum and the nearest charged particle be less than 20°. Additionally, the event is reclustered into minijets with the JADE algorithm [18] using $y = (2/\sqrt{s})^2$. The energy of the most energetic minijet, presumably the decay of a tau lepton, must be smaller than 8 GeV.

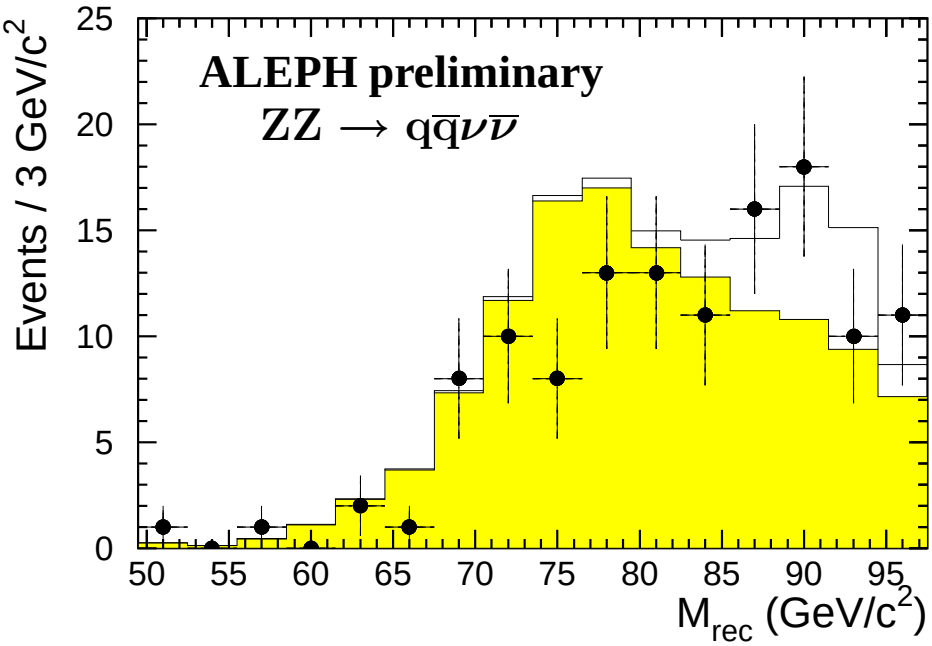

Figure 5: The distribution of masses for the $\mathrm{q\overline{q}}\nu\overline{\nu}$ channel. The grey region is the expected contribution from the background and the hollow region that from the $\mathrm{ZZ}\,\mathcal{NC}2$ signal.

To remove events from the $\mathrm{e^+e^-} \to \mathrm{We}\nu$ and $\mathrm{e^+e^-} \to \mathrm{Ze^+e^-}$ processes which have a detected final state electron near the beamline, the analysis requires that the energy in a cone of 12° around the beamline must be smaller than $2\%\,\sqrt{s}$. To remove events which have a missing momentum near the beamline and may be poorly measured, the polar angle of the missing momentum must point into the detector, $\theta_{\not p} > 25^\circ$. Figure 5 shows the reconstructed mass distribution with all cuts up to this point applied.

Because the mass of the Z boson is known, the mass information can be used effectively to reject much of the background. As for the other channels, an elliptical mass cut of "radius"

$$r^2 = \left(\frac{m_{\mathrm{rec}} - m_{\mathrm{Z}}}{\sigma_{m_{\mathrm{rec}}}}\right)^2 + \left(\frac{\not{M} - m_{\mathrm{Z}}}{\sigma_{\not M}}\right)^2$$

is used, where $\sigma_{m_{\mathrm{rec}}} = 3.1\ \mathrm{GeV}/c^2$ and $\sigma_{\not M} = 8.5\ \mathrm{GeV}/c^2$ are the approximate resolutions. Selected events have $r < 2$. The quantity m_{rec} is the invariant mass of the two jets with the missing mass constrained to m_{Z}.

The performance of this selection is shown in Table 1. The numbers in this table have been corrected for unsimulated accelerator backgrounds which increase the energy near the beamline; this effect was studied using random triggers. Half of the correction is used as an estimate of the systematic uncertainty. Similarly, the jet kinematics are corrected to make them better correspond to those observed in the data. Again, half of this correction is used as the systematic uncertainty. The systematic uncertainties also include uncertainties from the Z branching fractions, background production cross sections, and the limited statistics of the Monte Carlo samples. As the uncertainty on the luminosity is correlated between all channels it is included only in the combination. Adding these uncertainties in quadrature gives total relative uncertainties of 2% and 5% on the signal and background, respectively. For the efficiency, all of the

sources contribute approximately equally; for the background, the limited Monte Carlo statistics dominate.

4.3.2 Neural Network Selection

After preselection, a 12-variable neural network is employed to distinguish signal events from background. Four of the variables used in the neural net analysis (acoplanarity, minijet energy, direction of missing momentum, and energy within a 12° cone around the beamline) are shared with the cut analysis. Additionally, the neural network analysis uses the reconstructed Z mass directly instead of the elliptical mass used for the cut analysis. This analysis also includes two b-tagging variables; although only a fraction of events have a $\mathrm{b\bar{b}}\nu\overline{\nu}$ final state, the use of a neural network makes effective use of the b-tag possible. In addition, acolinearity, the visible energy beyond 30° of the beamline, the energy within a 30° wedge of the direction of the missing momentum, the z-component of the momentum, and the missing mass are used as variables. The output of the neural network is shown in Fig. 4.3.2 for Monte Carlo simulation and for data. Only events with a network output greater than 0.5 are used for the cross section calculation. The selection's performance is summarized in Table 1.

Systematic uncertainties include effects from Monte Carlo statistics, b-tagging uncertainties, and cross section uncertainties on background processes. The b-tagging systematics are estimated by reweighting the data with a function from comparison of Z-peak Monte Carlo simulation and data. The relative systematic errors on signal and background are 1% and 3%, respectively. The errors on the $\mathrm{q\bar{q}}$ and WW cross section are treated as correlated errors in the final combination.

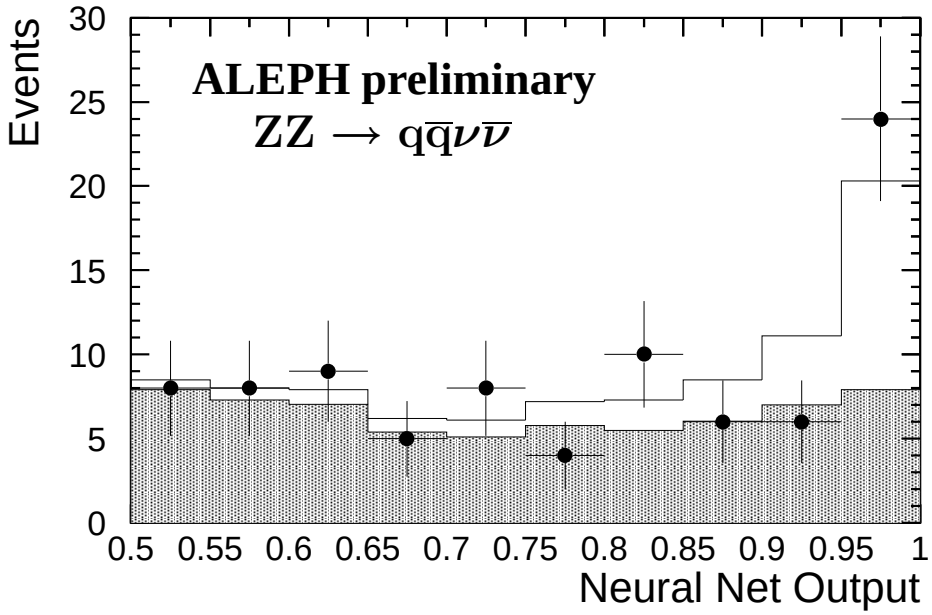

Figure 6: Neural network output from the $\mathrm{q\bar{q}}\nu\overline{\nu}$ selection for data and Monte Carlo simulation. The grey histogram shows the expected background, and the hollow histogram shows the expected $\mathcal{NC}2$ signal.

4.4 $\mathrm{Z} \to \ell^+\ell^-\nu\overline{\nu}$ Final States

Despite its small contribution to the total ZZ cross section, a dedicated selection has been devised for the $\ell^+\ell^-\nu\overline{\nu}$ channel.

The preselection requires events which have exactly two identified electrons or muons and no other reconstructed charged particles. These leptons must have the same flavour and opposite charge. The fraction of the total energy deposited in the central part of the detector, f_{30°, must be approximately half the total centre-of-mass energy, $0.4 < f_{30^\circ} < 0.6$. The acoplanarity of the two leptons must be less than 178°. For electron pair events, 49 ± 2 events are expected and 43 observed; for muon pair events, 13.2 ± 0.3 events are expected and 10 observed.

Cuts on other kinematic quantities further suppress the background. The invariant mass of the leptons and of the missing mass are required to be within an ellipse of $r < 1.7$ defined as above with $\sigma_{\not{M}} = 3.3\ \mathrm{GeV}/c^2$ and $\sigma_{m_{\ell\ell}} = 2.5\ \mathrm{GeV}/c^2$. The missing momentum must point away from the beamline, $\theta_{\not{p}} > 6.7^\circ$, and the total energy not associated with the leptons must be less than 5.6 GeV.

The performance of this selection is summarized in Table 1. For the efficiency, the systematic uncertainty is 5% with equal contributions from the Z branching fractions and the Monte Carlo statistics. For the background, the uncertainty is 17% dominated by the limited Monte Carlo statistics. The correlated uncertainty of 2% on the WW cross section gives a 1.8% correlated systematic uncertainty for this channel.

4.5 $\mathrm{Z} \to \tau\tau\mathrm{q}\overline{\mathrm{q}}$ Final States

In the neural network based selection, a dedicated analysis selects events with $\mathrm{Z} \to \tau^+\tau^-$ and $\mathrm{Z} \to \mathrm{q}\overline{\mathrm{q}}$ with a higher efficiency than the cut based 4-jet selection.

Hadronic events are selected by requiring at least 8 good charged tracks and an event charged energy greater than $0.2\sqrt{s}$. Background from WW and ZZ events with electron or muon decays is suppressed by rejecting events having an identified lepton with energy greater than $0.25\sqrt{s}$. Radiative returns to the Z peak, characterized by high missing energy and high missing momentum, are rejected by requiring $|p_z + E_{\mathrm{miss}}| < 1.8\gamma_{\mathrm{peak}}$, where p_z and E_{miss} are respectively the missing momentum and missing energy. To further reject radiative returns, events are also rejected if the event p_z is greater than $0.6\gamma_{\mathrm{peak}}$.

Events passing the preselection cuts are clustered into *minijets* having invariant masses consistent with m_τ. The τ candidates are selected from these minijets using a series of quality cuts based on multiplicity, isolation, and momentum. To be considered a τ candidate, a minijet must have one, two, or three charged tracks with momenta larger than $1\ \mathrm{GeV}/c$. If the minijet has three charged tracks, it must be of unit charge; if the minijet has two charged tracks, the minijet charge is the charge of the track with higher momentum. The minijet isolation angle, defined as the half-angle of the largest cone around the minijet direction containing no more than 5% of the total event energy outside the cone, must be larger than 15 degrees. Finally, the energy of a two- or three-prong minijet must be greater than $12.5\ \mathrm{GeV}/c$, while a one-prong minijet composed of less than 80% charged energy must have an energy greater than $7.5\ \mathrm{GeV}/c^2$. If the one-prong minijet is an identified electron or muon, no momentum cut is made, allowing in this case for the two expected neutrinos.

Only events with at least two τ candidates are further considered. At least one of the τ minijets must have exactly one prong, and the two minijets must have opposite charge. The

rest of the event is clustered into two jets using the Durham algorithm. All four jets in the event are rescaled using an overconstrained kinematic consistency fit in which the jet directions are fixed and the minijet masses are set to m_τ. The fit estimator χ^2 is calculated from energy-momentum conservation, the hadronic jet resolutions, and the difference between the two fitted dijet masses. This has the effect of constraining the dijets to equal masses. In no case are the hadronic jets allowed to rescale to less than 75% of their measured momenta. A typical event may have several possible combinations of potential τ minijet candidates; only the combination with the smallest calculated kinematic χ^2 is further considered.

A 5-variable neural network selects ZZ events from preselected events. Because the τ leptons decay with one or two neutrinos, the event transverse momentum p_T is input to discriminate against background events without missing energy.

The fit estimator provides a measure of the event's kinematic consistency with ZZ signal. The sum of the τ candidates' isolation angles and the sum of the τ candidates' transverse momenta with respect to their nearest hadronic jet ensure events contain well-isolated τ jets. Finally, the reconstructed Z mass, when combined with the implicit equal fit constraint, helps discriminate between $\mathcal{NC}2$ events and background. Events with a network output greater than 0.77 are selected for the cross section calculation. The performance of this selection is summarized in Table 1.

The systematic variables include effects from errors on reconstructed jet energies and angles, uncertainties in Standard Model cross sections, and Monte Carlo statistics. The relative systematic errors for signal and background are 3.0% and 10.8%. The error for signal is distributed equally among the sources, while the background error is dominated by limited Monte Carlo statistics.

5 Combination of Channels

Table 1 summarizes the efficiencies, numbers of events observed, etc. for all of the channels. A maximum likelihood fit determines the $\mathcal{NC}2$ cross section for the $\mathrm{e^+e^-} \rightarrow \mathrm{ZZ}$ process by combining the information from all of the channels. For the neural-network based analysis, a binned likelihood is used for the $\mathrm{q\overline{q}q\overline{q}}$ and $\mathrm{q\overline{q}\nu\overline{\nu}}$ channels where the shape of the neural-network distribution is used; for the other channels and for the cut-based analysis, only the total numbers of events are used in the likelihood.

The expected relative statistical uncertainties on the 188.6 GeV cross section measurements of 19.7% and 18.0% for the cut-based and neural-network based analyses, respectively, was determined with toy Monte Carlo experiments. The systematic uncertainty was determined by adding a Gaussian smearing to the efficiencies and background estimates in the toy Monte Carlo experiments and the change in the total error observed.

Correlated contributions to the total systematic uncertainty of the measurement are the luminosity (0.5%) and the uncertainties in the WW and $\mathrm{q\overline{q}}$ cross sections. The total relative systematic uncertainties are 4% and 6% for the cut-based and neural-network based analyses, respectively.

Table 1: Summary of the efficiencies, expected ZZ $\mathcal{NC}2$ and backgrounds, numbers of observed events, and the measured cross sections for each channel. The efficiency $\epsilon_\circ$ includes all branching fractions. (The symbol ℓ denotes only electrons and muons.)

	$\epsilon_\circ$ (%)	ϵ (%)	$N_{\rm bkg}$	$N_{\rm ZZ}^{\rm SM}$	$N_{\rm obs}$	$\sigma_{\mathcal{NC}2}$ (pb)
$\ell\ell$XX‡	7.77 ± 0.10	$76.7\ \pm0.5$	$1.1\ \pm0.3$	8.8	12	$0.80\pm^{0.28}_{0.23}$
$q\overline{q}q\overline{q}$ (b)*	7.31 ± 0.09	$14.6\ \pm0.2$	$3.8\ \pm0.4$	8.3	14	$0.80\pm^{0.32}_{0.27}$
$q\overline{q}q\overline{q}$ (non-b)*	14.11 ± 0.12	$27.4\ \pm0.2$	$60.0\ \pm1.4$	16.0	69	$0.36\pm^{0.35}_{0.32}$
$q\overline{q}q\overline{q}^\dagger$	15.20 ± 0.60	$\pm$	$19.7\ \pm1.8$	17.2	32	$0.58\pm^{0.22}_{0.19}$
$q\overline{q}\nu\overline{\nu}^*$	13.26 ± 0.12	$47.2\ \pm0.3$	$13.0\ \pm0.6$	15.0	30	$0.74\pm^{0.25}_{0.22}$
$q\overline{q}\nu\overline{\nu}^\dagger$	22.30 ± 0.20	$\pm$	$65.0\ \pm2.0$	25.3	88	$0.65\pm^{0.22}_{0.20}$
$\ell\ell\nu\overline{\nu}^\ddagger$	1.20 ± 0.04	$50.3\ \pm1.5$	$1.5\ \pm0.3$	1.4	1	$-0.26\pm^{0.66}_{0.30}$
$\tau\tau q\overline{q}^\dagger$	1.96 ± 0.06	$\pm$	$1.5\ \pm0.2$	2.2	3	$0.44\pm^{0.62}_{0.41}$

* cut analysis
† NN analysis
‡ both analyses

The measured cross sections at $\sqrt{s} = 188.6\ \mathrm{GeV}$ are

$$\sigma_{\mathcal{NC}2} = 0.69 \pm {}^{0.13}_{0.12}\,(\mathrm{stat.}) \pm 0.03\,(\mathrm{syst.})\ \mathrm{pb}$$

and

$$\sigma_{\mathcal{NC}2} = 0.64 \pm {}^{0.12}_{0.11}\,(\mathrm{stat.}) \pm 0.04\,(\mathrm{syst.})\ \mathrm{pb}$$

for the cut-based and neural-network based analyses, respectively, compared to the Standard Model expectation of 0.65 pb. Table 1 shows the cross section for each channel individually.

The cut-based analysis has also been applied to the 1997 data sample. The measured cross section is

$$\sigma_{\mathcal{NC}2} = 0.11 \pm {}^{0.16}_{0.11}\,(\mathrm{stat.}) \pm 0.04\,(\mathrm{syst.})\ \mathrm{pb}\,.$$

at a centre-of-mass energy of $\sqrt{s} = 182.7\ \mathrm{GeV}$ compared to the Standard Model expectation of 0.26 pb.

For the "NN" analysis, the cross section is extracted similarly except in the $q\overline{q}q\overline{q}$ and $q\overline{q}\nu\overline{\nu}$ channels, the neural network output distribution is used for a binned likelihood calculation. The $q\overline{q}q\overline{q}$ distribution is divided into six bins between 0.7 and 1.0, while the $q\overline{q}\nu\overline{\nu}$ is divided into ten bins between 0.5 and 1.0. The expected uncertainty after combining all channels is 18.0%. The results from the likelihood fit are presented in Table 1.

For the neural-network based analysis, the overlaps between channels are explicitly removed. About 0.2% of the events in the $q\overline{q}q\overline{q}$ selection are $\tau\tau q\overline{q}$ events in which a 3-prong τ is misidentified as a quark jet, and about 0.5% are $q\overline{q}\mu^+\mu^-$ events. To ensure the exclusivity of the analyses, the overlapping signal and background are explicitly subtracted from the $q\overline{q}q\overline{q}$ results. For the given signal and background numbers, toy simulated experiments are generated, and the expected uncertainty on the cross section measurement is derived from the width of the extracted cross section distribution.

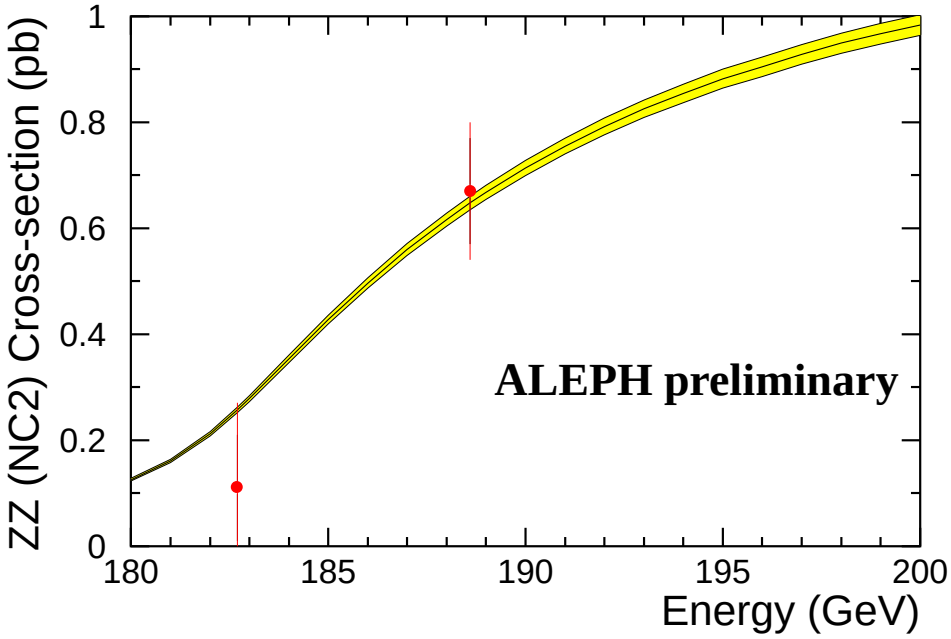

Figure 7: The measured $\mathcal{NC}2$ cross sections compared to the expected Standard Model cross section. The shaded area represents the theoretical uncertainty ($\pm 2\%$) on the YFSZZ calculations.

6 Cross Checks

6.1 Four-fermion Interference

The PYTHIA Monte Carlo generator does not fully simulate the interference between all of the four-fermion diagrams. This potentially biases the cross section measurement presented here. Using EXCALIBUR, which does include the interference, to generate samples for the signal and four-fermion backgrounds and rerunning the cut-based analysis yields a relative difference in the cross section measurement of -1%. This is a negligible effect when compared to the magnitude of the statistical error.

6.2 Biases from New Physics

For a Higgs boson with a mass near that of the Z boson, the Higgsstrahlung process $\mathrm{e^+e^-} \to h\mathrm{Z}$ has a production cross section, 0.3 pb, which is comparable to the ZZ production cross section. In this case, the measured cross section from the b-selection alone would be significantly larger than the others. Table 1 shows that this is not the case. Moreover, a combination of the cut-based channels without the b-selection and with specific cuts removing b-quark jets is performed producing a cross section $\sigma = 0.63 \pm 0.16$ pb, consistent with the above value.

6.3 Correlations Between the WW and ZZ Cross Sections

ALEPH has observed a large statistical fluctuation downward of the observed WW cross section in the 1998 data sample [17]. As WW production is a large, common background for all

channels this could have a sizeable effect on the ZZ cross section measurement. Two checks are done. First, the expected WW backgrounds of the four-quark channels of the cut-based analysis were reduced by 10% and the combination redone. This leads to a $+3.5\%$ relative change in the measured cross section. Second, both the ZZ and WW cross sections were simultaneously fit in the cut-based likelihood combination. As expected, the measured ZZ cross section increases to 0.80 ± 0.16 pb but remains consistent with the above value. The fitted WW cross section 12.4 ± 3.5 pb is consistent with the lower WW cross section already observed.

7 Conclusions

Two analyses have measured the ZZ cross section using the data taken in 1998. Both analyses agree with each other and with the Standard Model value of 0.65 pb. The ZZ production cross section is taken to be the arithmetic average of the above two measurements

$$\sigma_{\mathrm{ZZ}} = 0.67 \pm 0.13\,(\mathrm{stat.}) \pm 0.04\,(\mathrm{syst.})\,\mathrm{pb}\,.$$

at $\sqrt{s} = 188.6$ GeV.

Additionally, the cut-based analysis has been applied to the 1997 data sample yielding a measurement of

$$\sigma_{\mathrm{ZZ}} = 0.11 \pm {}^{0.16}_{0.11}\,(\mathrm{stat.}) \pm 0.04\,(\mathrm{syst.})\,\mathrm{pb}\,.$$

at a centre-of-mass energy of $\sqrt{s} = 182.7$ GeV.

Figure 7 compares the measured values with the Standard Model expectation and shows the good agreement between the Standard Model expectation and the measurements.

Acknowledgements

The authors would like to thank W. Płaczek for his help with the YFSZZ generator. It is also a pleasure to congratulate our colleagues from the CERN accelerator divisions for the successful operation of LEP. We are indebted to the engineers and technicians in all our institutions for their contributions to the excellent performance of ALEPH. Those of us from non-member countries thank CERN for its hospitality.

References

[1] ALEPH Collaboration, *"ALEPH: A Detector for Electron-Positron Annihilations at LEP."*, *Nucl. Instrum. Methods* **A294** (1990) 121.

[2] ALEPH Collaboration, *"Performance of the ALEPH detector at LEP."*, *Nucl. Instrum. Methods* **A360** (1995) 481.

[3] ALEPH uses a right-handed coordinate system defined such that the z-axis points in the direction of the electrons and the x-axis points toward the centre of the LEP ring.

[4] S. Jadach, W. Płaczek, and B.F.L. Ward, *Phys. Rev.* **D56** (1997) 6939.

[5] The following electroweak parameters were used: $m_{\rm Z} = 91.1888$ GeV/c^2, $\Gamma_{\rm Z} = 2.4974$ GeV/c^2, $m_{\rm W} = 80.35$ GeV/c^2, $\Gamma_{\rm W} = 2.09483$ GeV/c^2, $\sin^2(\theta_W) = 0.230341$, $1/\alpha(m_{\rm Z}) = 128.07$, and $\alpha_s(m_{\rm Z}) = 0.12$.

[6] T. Sjöstrand, *The PYTHIA 5.7 and JETSET 7.4 Manual*, LU-TP.95/20 and CERN-TH.7112/93.

[7] F.A. Barends, R. Pittau, and R. Kleiss, *Comput. Phys. Commun.* **85** (1995) 437.

[8] T. Ishikawa *et al.*, KEK-92-19 (1993).

[9] M. Skrzypek *et al.*, *Comput. Phys. Commun.* **94** (1996) 216.

[10] S. Jadach and Z. Wąs, *Comput. Phys. Commun.* **36** (1995) 191.

[11] S. Jadach, W. Płaczek, and B.F.L. Ward, *Phys. Lett.* **B390** (1997) 298.

[12] R. Engel, *Z. Phys.* **C66** (1995) 203; R. Engel and J.Ranft, *Phys. Rev.* **D54** (1996) 4144.

[13] ALEPH Collaboration, *"Search for the Neutral Higgs Bosons of the Standard Model and the MSSM in* $\rm e^+e^-$ *Collisions at* $\sqrt{s} = 188.6$ GeV.", ALEPH 99-007 (CONF 99-003) available from http://alephwww.cern.ch/; ALEPH Collaboration, *Phys. Lett.* **B447** (1999) 336; ALEPH Collaboration, *Phys. Lett.* **B440** (1998) 419, *erratum Phys. Lett.* **B447** (1999) 355.

[14] ALEPH Collaboration, , *"Heavy flavour production and decay with prompt leptons in the ALEPH detector."*, *Z. Phys.* **C62** (1994) 179.

[15] N. Brown and W.J. Stirling, *Phys. Lett.* **B252** (1990) 657; S. Catani *et al.*, *Phys. Lett.* **B269** (1991) 432; N. Brown and W.J. Stirling, *Z. Phys.* **C53** (1992) 629.

[16] ALEPH Collaboration, , *"Measurement of the* W *mass in* $\rm e^+e^-$ *Colisions at* $\sqrt{s} = 189$ GeV.", *Phys. Lett.* **B453** (1999) 121.

[17] ALEPH Collaboration, *WW cross section and W branching ratios at* $\sqrt{s} = 189$ GeV.", ALEPH 99-020 (CONF 99-015), available from http://alephwww.cern.ch/.

[18] JADE Collaboration, W.Bartel *et al., Z. Phys.* **C33** (1986) 23; S.Bethke *et al., Phys. Lett.* **B213** (1988) 235.